crystals

MDPI

Article

Crystallographic Data Collection Using a Multilayer Monochromator on an Undulator Beamline at the Shanghai Synchrotron Radiation Facility

Chenyu Zhang [1,2,†], Qin Xu [1,3,†], Weiwei Wang [1,3], Miao Liang [1,2], Li Yu [1,2], Minjun Li [1,2], Zhimin Zhu [1,2], Liqing Huang [1,2], Qianhui Li [1,2], Feng Yu [1,3], Yuzhu Wang [1,3], Huan Zhou [1,3,*] and Qisheng Wang [1,2,3,*]

1 Shanghai Institute of Applied Physics, Chinese Academy of Sciences, Shanghai 201800, China; zhangchenyu@sinap.ac.cn (C.Z.); xuq@sari.ac.cn (Q.X.); wangww@sari.ac.cn (W.W.); liangmiao@sinap.ac.cn (M.L.); yuli@sinap.ac.cn (L.Y.); limj@sari.ac.cn (M.L.); zhuzhimin@sinap.ac.cn (Z.Z.); huangliqing@sinap.ac.cn (L.H.); liqianhui@sinap.ac.cn (Q.L.); yufeng@sinap.ac.cn (F.Y.); wangyz@sari.ac.cn (Y.W.)
2 University of Chinese Academy of Sciences, Beijing 100049, China
3 Shanghai Synchrotron Radiation Facility, Shanghai Advanced Research Institute, Chinese Academy of Sciences, Shanghai 201204, China
* Correspondence: zhouhuan@sari.ac.cn (H.Z.); wangqs@sari.ac.cn (Q.W.)
† These authors contributed equally to this work.

Abstract: To resolve photons hungry for weak diffraction samples by the crystallographic method, a double-multilayer monochromator (DMM) was employed on an undulator beamline (BL17UM) at the Shanghai Synchrotron Radiation Facility (SSRF) to provide a focused sub-micron beam with high brightness for macromolecular crystallography experiments. High-quality crystallographic datasets from model protein crystal samples were collected and processed by an existing crystallographic program for structure solution and refinement. The data quality was compared with datasets from a normal silicon crystal monochromator to evaluate the bandwidth of the DMM effect on these crystallographic data. This experiment demonstrates that multilayer optics on an undulator beamline may play a valuable role in satisfying the demands of structure-related research, which requires novel methods.

Keywords: double-multilayer monochromator; macromolecular crystallography; room temperature crystallography

Citation: Zhang, C.; Xu, Q.; Wang, W.; Liang, M.; Yu, L.; Li, M.; Zhu, Z.; Huang, L.; Li, Q.; Yu, F.; et al. Crystallographic Data Collection Using a Multilayer Monochromator on an Undulator Beamline at the Shanghai Synchrotron Radiation Facility. *Crystals* **2024**, *14*, 199. https://doi.org/10.3390/cryst14020199

Academic Editor: Ki Hyun Nam

Received: 12 January 2024
Revised: 9 February 2024
Accepted: 13 February 2024
Published: 19 February 2024

1. Introduction

Macromolecular X-ray crystallography (MX) is the study of biomolecules using diffraction phenomena to determine their structure. The diffraction intensity is directly related to the incident X-ray and the sample crystal. Therefore, several methods have been developed to obtain high-quality crystals in the wet lab. These include microbatch experiments, dialysis, free interface diffusion, microfluidics, and, notably, vapor diffusion, which stands out as the most extensively employed technique for crystallization [1]. Meanwhile, due to the relatively weak diffraction ability of biomolecules, the flux of the beam is a very important metric for such applications. Flux hunger is a persistent issue in this field [2]. Depending on the energy width of the X-ray, the experiment method can be mono or Laue [3]. The key distinction lies in the X-ray bandwidth. The mono method employs a narrow, practically monochromatic bandwidth, while the Laue method utilizes nearly the full energy bandwidth (white beam) of the source [4]. Thus, worldwide, the MX beamlines have prolonged efforts to offer higher-brightness X-ray beams for data collection. Monochromatic crystallography has overwhelmingly dominated structural studies, accounting for over 99% of the solved structures. In contrast, the application of Laue crystallography has been limited due to its inherent experimental and data processing complexities [5]. To meet the

stringent requirements for the photon flux density, the double-multilayer monochromator (DMM) has garnered attention and led to the identification of practical applications in addressing such challenges. DMMs have been used to improve the flux density in second-generation synchrotrons, such as the CHESS light source and DORIS III storage ring (DESY/Hamburg) [3,6]. However, in third-generation synchrotron sources, DMMs are primarily employed in applications related to small-angle scattering and imaging [7]. Recently, researchers have explored the usage of DMMs for protein crystal diffraction experiments in third-generation synchrotrons [8].

In this study, we report the detailed crystallographic data collection on an undulator beamline using a DMM. The data were carefully analyzed using standard crystallographic software and compared with data from the same protein that was collected using an Si(111) monochromator. The detailed evaluation of different aspects showed that the data quality was quite similar.

Determining the crystal structure at or above ambient temperature is crucial to understanding protein function, allostery, and ligand/drug binding [9]. Recent research has highlighted differences in conformational responses to radiation damage and revealed challenges in obtaining such structures, especially with small or fragile crystals such as those of membrane proteins, large complexes, or viruses [10]. Serial crystallography (SX), X-ray free-electron lasers (XFELs), or synchrotron X-rays allow for the determination of macromolecular structures at room temperature while minimizing radiation damage [11]. SX, with a pump probe or mix-and-inject experiments, can provide insights into the time-resolved molecular dynamics of the target molecule [10,12]. Overall, it offers a more reliable understanding of biological macromolecular structures and detailed molecular mechanisms compared to conventional macromolecular crystallography [13]. XFELs produce intense X-rays with ultrashort pulse widths, making serial femtosecond crystallography (SFX) suitable for time-resolved studies with short time delays (fs–ns) [11,14]. However, the limited beam-time availability on XFELs has led to the alternative approach of serial synchrotron crystallography (SSX) using a synchrotron source [15]. At the Shanghai Synchrotron Radiation Facility (SSRF), we collected diffraction data of a model protein lysozyme using a DMM at room temperature and successfully determined its structure. Structural analysis revealed that the structure was identical to that resolved at 100 K using a Si(111) monochromator. This lays the foundation for future serial crystallography experiments using DMM at the SSRF.

An improved understanding of the protein crystal structure has played a crucial role in drug development in the past few decades. By resolving the high-resolution crystal structure of proteins, scientists have gained in-depth insights into the biological functions and molecular interactions of proteins, laying the foundation for targeted drug design [16]. In recent years, with the continuous advancement of structural biology techniques, significant progress has been made in drug development [17]. Through protein crystallography, scientists have elucidated the precise binding modes between drugs and target proteins, providing critical information for drug design. Combined with computational methods, such structure-guided design has allowed for more efficient screening and design of potential drug molecules [18]. In this study, we successfully determined the crystal structures of the SARS-CoV-2 Mpro and the ZIKV NS2B/NS3 proteases using a DMM to evaluate the application of DMMs in drug discovery. Through structural comparison, the viral drug target structures resolved with the DMM were found to be essentially consistent with those previously resolved using a conventional monochromator.

At the SSRF, there are already five MX beamlines open to users [19,20]. BL17UM is a newly established MX beamline at the SSRF. The primary focus of this paper is to provide valuable insights for scientists utilizing the DMM at this beamline for data collection. We utilized the DMM at this beamline to collect crystal diffraction data for various proteins, including the model protein lysozyme, SARS-CoV-2 Mpro, and ZIKV NS2B/NS3. Their structures were successfully determined using conventional methods. Additionally, data were collected for the model protein at room temperature using the DMM, and its struc-

ture was successfully resolved. These datasets can contribute to future research in drug development and serial crystallography using the DMM at this beamline.

2. Materials and Methods

2.1. Performance of the DMM

The DMM on the beamline BL17UM was homemade by the SSRF and Tongji University. The materials for the two strips included Ru/C and W/Si to cover the energy ranging within 10−18 keV and 18−25 keV, respectively [21]. Using the analysis of crystal Si(111) at the sample position, the energy resolution of the beam from the DMM was 0.775% at an energy of 12 keV. The equation $\frac{\Delta E}{E} = \sqrt{(\Delta\varphi_p)^2 + (\Delta\varphi_d)^2}ctg\theta \approx (\Delta\varphi_r)ctg\theta$ was used to calculate the energy resolution (Figure 1).

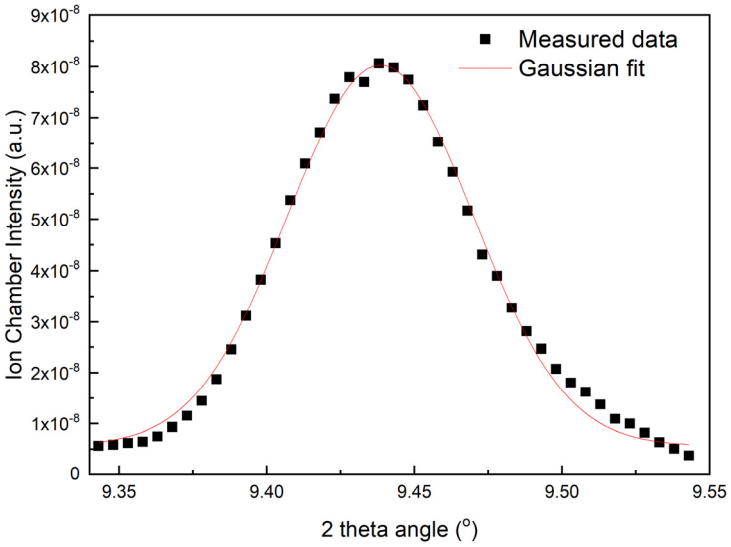

Figure 1. Measuring the photon energy resolution using an Si(111) crystal.

2.2. Sample Preparation

Lysozyme was crystallized following a previously described method. The lysozyme powder was directly dissolved in deionized water. The concentration of lysozyme used for crystal growth was 25 mg/mL. The crystal growth condition was 100 mM sodium acetate (pH 4.6) and 6% sodium chloride, and crystals were grown using the hanging-drop method. Crystals of sizes ranging from 0.02 to 0.05 mm were obtained overnight and were utilized in the subsequent experiments. Under the aforementioned conditions, lysozyme crystallizes in the tetragonal space group $P4_32_12$ [22].

The SARS-CoV-2 Mpro gene was inserted into the pET-15b vector, and the resulting plasmid was introduced into BL21 (DE3) cells for protein expression. *E. coli* carrying the Mpro gene were extracted from the glycerol stock and were inoculated into an LB medium using kanamycin (25 µg/mL) as a selection marker. Then, the cells were incubated overnight at 37 °C. Next, 1% (*v*/*v*) of the overnight primary culture was inoculated into 1 L of LB medium containing kanamycin and cultured at 37 °C. The growth was monitored by measuring the absorbance at 600 nm. When the OD reached 0.4–0.6, the culture was induced by adding 1 mM IPTG, cultured for an additional 4 h at 37 °C, and, finally, the cells were harvested using a centrifuge at 4 °C and 6000 rpm. The cells were sonicated in ice-cold lysis buffer (50 mM Tris-HCl, pH 8.5, 100 mM NaCl) and the lysate was centrifuged at 10,000 rpm, 30 min, 4 °C. After purification with a Ni-NTA column (GE Healthcare, Chicago, IL, USA) and subsequently conducting size-exclusion chromatography (SuperdexTM 200 pg, GE Healthcare), the eluted Mpro protein was concentrated to 10 mg/mL for crystallization. Crystallization was carried out at 18 °C using the hanging-drop vapor diffusion method

by combining equal volumes (1:1 µL) of the protein and reservoir solution. Crystals were successfully obtained under the conditions of 25% PEG800, 100 mM MES, and pH 5.5 [23].

The ZIKV NS3 protease gene (residues 1–177) and NS2B (residues 46–99) were cloned into the pET-15b vector and transformed into E. coli strain BL21 (DE3) cells for expression, as in a previous report [24]. The cell pellets were resuspended in a buffer (containing 25 mM Tris, pH 8.5, 500 mM NaCl, 20 mM imidazole, 10% glycerol) for lysis. After centrifugation, the lysate was loaded onto a Ni-NTA column (GE Healthcare). NS2B/NS3 protein was eluted using a buffer with 250 mM imidazole, concentrated, and loaded onto a gel filtration column (Superdex 200 20/300 GL, GE Healthcare) equilibrated with a gel filtration buffer (25 mM Tris, pH 8.5, 150 mM NaCl, 5% glycerol). The eluted NS2B/NS3 protein was finally concentrated to 15 mg/mL for crystallization. NS2B/NS3 proteins were crystallized at 18 °C by hanging-drop vapor diffusion. Protein and reservoir solutions (0.2 M ammonium sulfate, 20% PEG 2000, 0.1 M sodium acetate trihydrate, pH 4.6) were combined in equal volumes (1 µL). Crystals usually appeared at five days. Before being flash-frozen in liquid nitrogen, the crystals were cryoprotected using the reservoir solution containing 20% glycerol.

2.3. Data Collection

The diffraction data were collected at the BL17UM station at the SSRF. The storage ring was operated at 3.5 GeV with a beam current of 220 mA in the top-up mode. When initiating crystallographic diffraction experiments, the energy was set to 13.422 keV in the DMM mode, the focused beam size was 0.69 × 0.58 μm^2, and the photon flux was 3.23×10^{12} phs/s. After switching to the Si(111) monochromator, the focused beam size was the same as the DMM mode, and the photon flux was 3.07×10^{11} phs/s. Owing to the high photon flux density, the data collection temperature was set as 100 K. The crystals were loaded in the Unipuck and mounted onto a diffractometer using a robotic arm. Data were collected from a tiny lysozyme crystal of 0.03 mm*0.02 mm*0.02 mm size using a Dectris Eiger2 X 16M detector with an exposure time of 0.02 s and 1 degree oscillation per image. For comparative purposes, a dataset was also collected using a Si(111) monochromator from a crystal of similar size at the same energy, with identical data collection parameters.

2.4. Data Processing

The diffraction images were visualized using Albula software (https://www.dectris.com/en/detectors/albula-software/, version ALBLA Viewer 4.1.3, accessed on 22 December 2023). The diffraction data were processed by using the XDS package [25].

2.5. Structure Determination

Molecular replacement methods in Phaser-MR within PHENIX were employed to solve the phasing problem. The model was developed using COOT [26], and subsequent structure refinement was carried out by using phenix.refinement in PHENIX [27,28]. Validation of the final structures was performed using MolProbity. The structural figures were created using PyMOL (https://pymol.org/, accessed on 1 October 2022).

3. Results

3.1. DMM and DCM Data Collection

The diffraction datasets exhibited Bragg peaks with a slightly elongated shape by utilizing DMM X-rays (Figure 2). Notably, the multilayer generated more reflections under the same conditions. The diffraction data were processed with XDS. Table 1 provides a summary of the data collection and processing parameters. The processed statistics indicate consistent values for multiplicity, the count of unique reflections, resolution limits, and completeness.

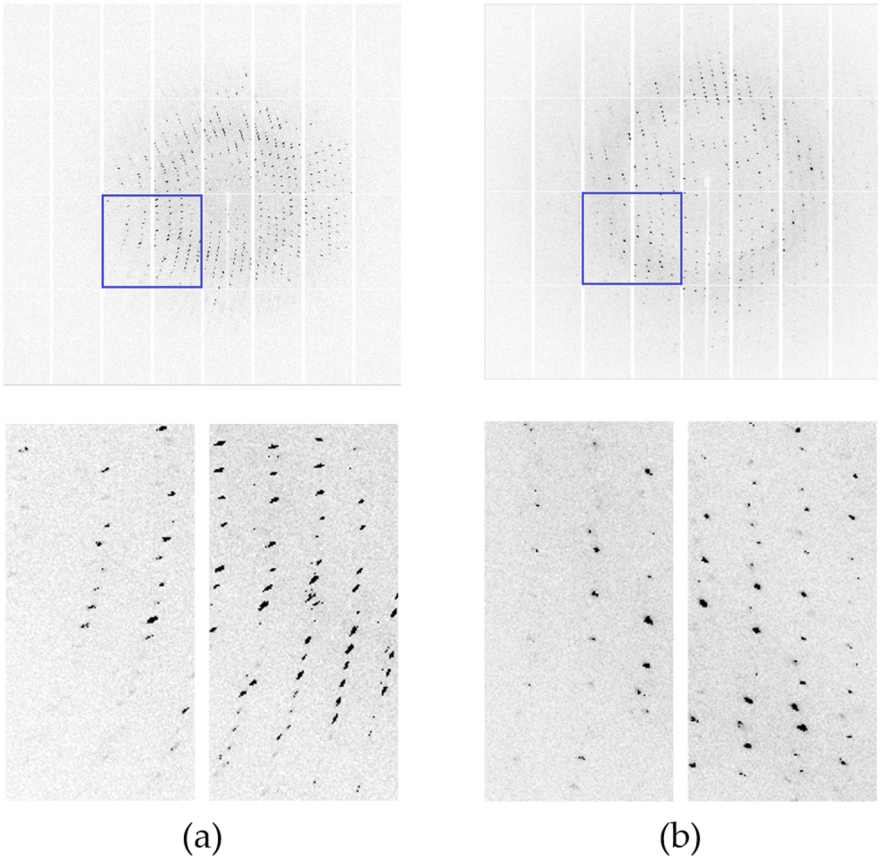

Figure 2. The blue box represents the enlarged region selected from the diffraction pattern. (**a**) The top image shows the diffraction image of lysozyme collected from the DMM at 100 K; the bottom image shows a close-up view of a specific region of the diffraction pattern, revealing a slight streaking. (**b**) The top image shows the diffraction image of lysozyme collected from the DCM at 100 K; the bottom image shows a close-up view of a specific region of the diffraction pattern, showing a relatively more circular pattern.

On average, the quality factor R_{meas} was more than 40% higher for the data obtained with Si(111) compared to that collected with the DMM. The difference was approximately 20% at the higher resolution shells.

The DMM data exhibited, on average, a signal-to-background ratio I/б(I) that was more than 85% higher than the Si(111) data. In the higher resolution shells, this difference exceeded 1.5 times.

Lysozyme is a common model protein with a molecular weight of 14.4 kDa, and it consists of 129 amino acid residues. We employed the molecular replacement method using Phaser-MR in Phenix software (Version 1.20.1-4487) to determine its initial phases. The initial model was obtained from a previously published high-resolution dataset, and the PDB entry was 2VB1. During processing, water molecules were removed, and all atoms were set as isotropic. A single satisfactory solution was identified and further refinement of the model led to notable improvement. Table 1 provides the R_{work}, R_{free}, and overall B factor after refinement.

The analysis reveals an approximately 5% higher R_{work} and a 16% higher R_{free} for the structure refined with data from Si(111) compared to the structure obtained from DMM data collection.

Table 1. Data collection and refinement statistics.

	100K-DCM-Lys	100K-DMM-Lys	RT-DMM-Lys	100K-DMM-Mpro	100K-DMM-NS2B/NS3
Resolution range (Å)	38.58–1.90 (1.94–1.90)	39.13–1.57 (1.59–1.57)	39.41–2.10 (2.16–2.10)	48.21–2.52 (2.62–2.52)	45.76–2.70 (2.83–2.70)
Space group	$P4_32_12$	$P4_32_12$	$P4_32_12$	C121	$P4_32_12$
Unit cell parameters					
a, b, c (Å)	77.16, 77.16, 36.85	78.26, 78.26, 36.81	78.82, 78.82, 37.70	45.42, 53.42, 113.91	59.74, 59.74, 213.53
α, β, γ (°)	90, 90, 90	90, 90, 90	90, 90, 90	90, 101, 90	90, 90, 90
Multiplicity	16.9 (9.8)	18.8 (18.2)	24.8 (24.8)	6.4 (6.3)	24.4 (23.9)
Completeness (%)	99.9 (98.7)	99.90 (97.1)	100.0 (100.0)	98.4 (96.3)	99.4 (95.6)
$\langle I/\sigma(I) \rangle$	16.6 (1.8)	30.90 (5.2)	20.2 (6.6)	4.7 (0.8)	16.1 (6.2)
Wilson B factors (Å^2)	32.30	17.77	13.98	51.06	31.18
Unique reflections	9250 (587)	16,608 (788)	7407 (585)	9012 (963)	11,424 (1419)
R_{meas}	0.28 (0.07)	0.15 (0.03)	0.29 (0.08)	0.79 (0.13)	0.22 (0.07)
$CC_{1/2}$	0.99 (0.87)	1.00 (0.94)	0.99 (0.93)	0.85 (0.43)	0.99 (0.96)
Reflections used in refinement	9216 (878)	16,564 (1599)	7376 (707)	8887 (758)	11,348 (1032)
R_{work}	0.20	0.19	0.19	0.25	0.18
R_{free}	0.25	0.21	0.24	0.30	0.25
Protein residues	129	129	129	300	387
RMS bonds (Å)	0.01	0.01	0.01	0.01	0.01
RMS angles (°)	1.07	1.11	0.97	0.46	0.97
Ramachandran plot (%)					
Favored	97.64	99.21	99.21	96.64	97.56
Allowed	2.36	0.79	0.79	3.02	2.17
Outliers	0.00	0.00	0.00	0.34	0.27
Overall B factors (Å^2)	41.06	23.62	24.88	57.15	35.34
PDB ID	8Y9W	8YA1	8YA4	8YA5	8Y9V

The values in parentheses are for the outermost shell. R_{free} is the R_{work} based on 5% of the data excluded from the refinement. $R_{meas} = \sum_{hkl} \sqrt{n/(n-1)} \sum_{i=1}^{n} | I_i(hkl) - \langle I(hkl) \rangle | / \sum_{hkl} \sum_i I_i(hkl)$, where $\langle I(hkl) \rangle$ is the mean intensity of a set of equivalent reflections. $R_{work} = \sum_{hkl} \| F_{obs} | - | F_{calc} \| / \sum_{hkl} | F_{obs} |$, where F_{obs} and F_{calc} are the observed and calculated structure factors, respectively. 100K-DCM-Lys represents the lysozyme data collection at 100 K using Si(111) monochromator; 100K-DMM-Lys represents the lysozyme data collection at 100 K using DMM; RT-DMM-Lys represents the lysozyme data collection at room temperature using DMM; 100K-DMM-Mpro represents the Mpro data collection at 100 K using DMM; 100K-DMM-NS2B/NS3 represents the NS2B/NS3 data collection at 100 K using DMM.

3.2. Room-Temperature Data Collection with DMM

Room-temperature data collection addresses cryocrystallography challenges effectively. While larger crystal volumes are needed, typically one or a few crystals will suffice. This eliminates the need to identify suitable cryoprotection and cryocooling conditions, allowing for broader screening with more cryoprotectant-free options. Advances in sample supports and loading tools have made it feasible to position each crystal in every drop within the X-ray beam without significant dehydration-induced non-isomorphism or background scatter. Fine slicing, smaller beam diameters, and reduced divergences have contributed to maximizing the diffraction signal-to-background ratio and achieving resolutions comparable to cryogenic temperatures.

A complete set of data were collected using DMM X-rays. Initially, conventional crystal retrieval tools were employed to fetch a lysozyme crystal of approximately 200 µm. Subsequently, the crystal was enclosed with a purchased loop sleeve to prevent dehydration during data collection. Due to the susceptibility of crystals to radiation damage at room temperature, each diffraction image was exposed for 0.02 s with a rotation of 1 degree. Only 180 diffraction images were collected, which was sufficient to resolve the lysozyme crystal

structure. The lysozyme crystal structure was determined using the molecular replacement method, and the relevant data processing and statistical structure parameters are provided in Table 1.

The lysozyme structure obtained through DMM data collection shows the clear visibility of all amino acids, including side chains in the electron-density maps. The quality of these maps is comparable to structures resolved using the conventional monochromator DCM (Figure 3a).

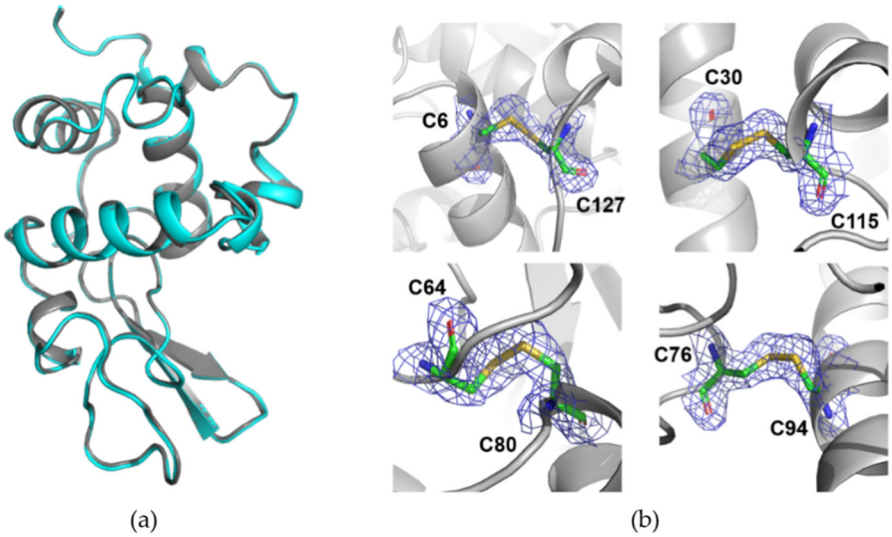

Figure 3. (**a**) Comparing the structure of lysozyme at room temperature using DMM (grey) and at 100 K using DCM (cyan). (**b**) 2mFo-DFc (marine mesh, 1.0) and mFo-DFc (green mesh 3.0, and red mesh 3.0) electron-density maps for the disulfide bonds (C6–C127, C30–C115, C64–C80, and C76–C94) of the lysozyme.

In lysozyme, four disulfide bonds are formed by eight cysteine residues (C6–C127, C30–C115, C64–C80, and C76–C94). The sulfur atoms in cysteine are relatively sensitive to radiation damage due to their higher atomic number, especially when lysozyme crystals are exposed to radiation exceeding a specific X-ray dose limit. To confirm the occurrence of radiation damage, the electron-density maps of 2mFo-DFc and mFo-DFc for the lysozyme disulfide bonds were analyzed, and significant negative electron-density maps were not observed (Figure 3b).

3.3. Data Collection of Mpro from SARS-CoV-2 with DMM

SARS-CoV-2 is a highly contagious coronavirus with a single-stranded positive-sense RNA genome [29]. Upon infection, the virus synthesizes 16 nonstructural proteins (nsps) as large polyproteins, namely pp1a and pp1ab, directly from its RNA genome [30]. During this process, among the 16 nsps, the main protease (Mpro or nsp5) plays a crucial role in hydrolyzing the polyproteins at 11 cleavage sites, releasing functional nsps essential for viral replication and transcription [31]. Due to its significance in the viral life cycle, Mpro has been identified as a potential drug target to combat SARS-CoV-2 [32].

Since the first structure of the SARS-CoV-2 Mpro was resolved at the SSRF, drugs or drug candidates based on the Mpro structure have been developed, and relevant drug development efforts are ongoing [33]. By using DMM, we have successfully solved the structure of Mpro, laying the groundwork for the future development of antiviral drugs against SARS-CoV-2.

The initial phase was obtained by molecular replacement and the final structure was obtained after several rounds of refinement. The structure exists as a dimer, and when compared with the Mpro structure previously resolved by DCM, the overall structures are quite consistent (Figure 4a). Simultaneously, we conducted a detailed comparison of their

active sites. In the Mpro structure resolved using DMM data collection, the electron density of the active site is very clear (Figure 4b).

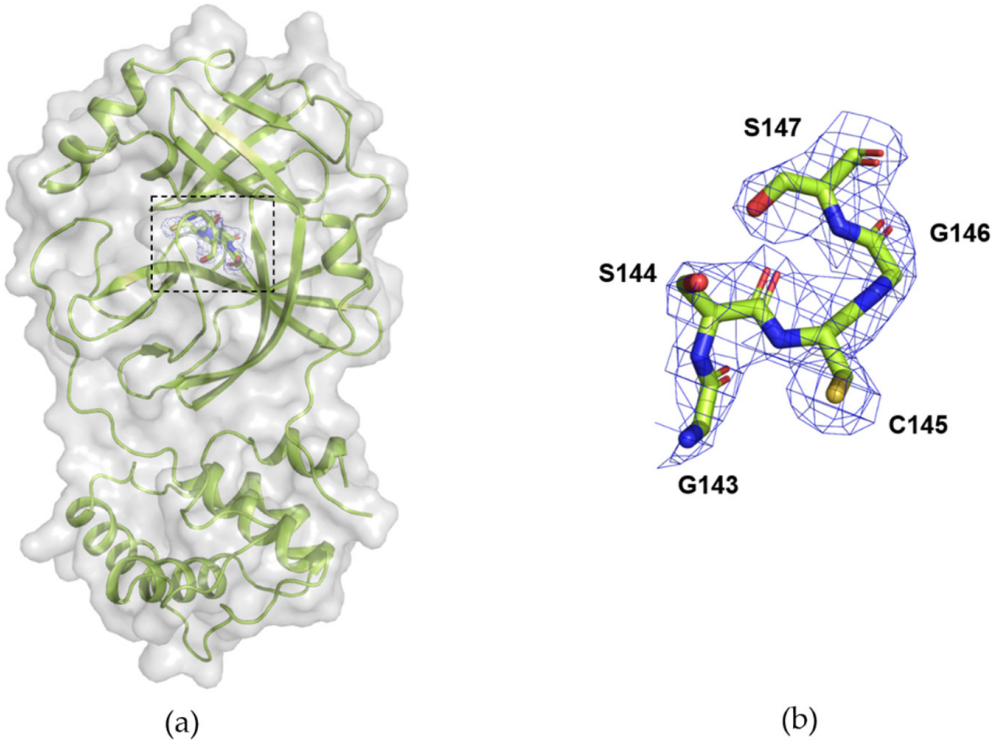

Figure 4. (**a**) Schematic representation of a protomer of the dimeric structure of Mpro, collected at 100 K using DMM. The active site is highlighted within the black box; (**b**) the 2mFo-DFc (marine mesh, 1.0) electron-density map for the active site and substrate binding region of Mpro. In the sticks, green represents carbon atoms, blue represents nitrogen atoms, red represents oxygen atoms, and orange represents sulfur atoms.

3.4. Data Collection of ZIKV NS2B/NS3 Protease with DMM

The Zika virus is a major health threat with no approved vaccine or treatment. The NS2B/NS3 protease in ZIKV is a key target for developing antiviral drugs. Similar to other flaviviruses, ZIKV possesses a positive-sense single-stranded RNA genome that codes for a polyprotein. The NS2B/NS3 protease, along with host cell proteases, cleaves this polyprotein into three structural proteins (C, prM/M, and E) and seven non-structural proteins (NS1, NS2A, NS2B, NS3, NS4A, NS4B, and NS5). NS3, a chymotrypsin-like serine protease, contains a catalytic triad (His51-Asp75-Ser135), while NS2B serves as a cofactor and collaborates with NS3 to create the substrate-binding site. The NS2B/NS3 protease is crucial for viral replication and is a promising target for antiviral interventions.

In order to collect crystal diffraction data on DMMs for future antiviral drug development, we also utilized the DMM to collect diffraction data of the NS2B/NS3 protease in ZIKV. The structure was resolved by molecular replacement, and a structural comparison revealed consistency with the structure resolved using DCM. Both the main chain and side-chain electron densities are clear. Figure 5 displays the electron-density map of the active site.

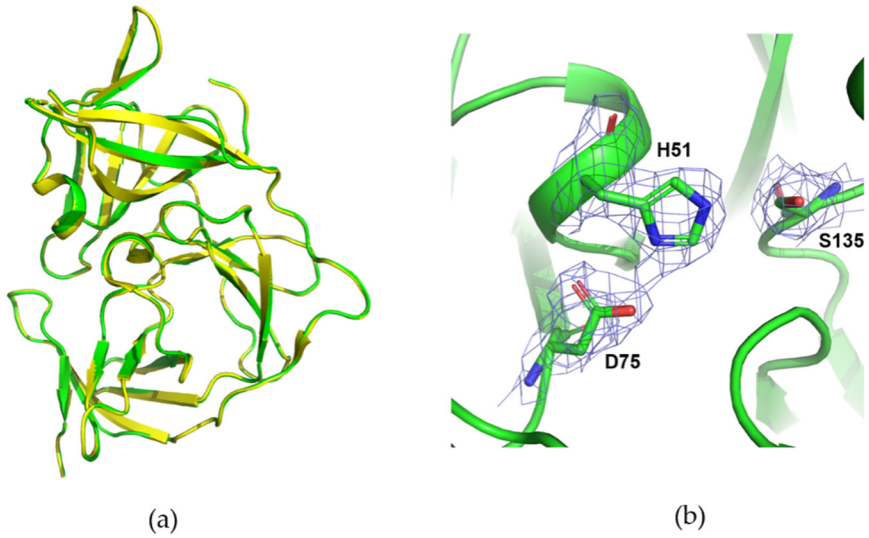

Figure 5. (**a**) Structure comparison of the NS2B/NS3 protease using DMM (green) and DCM (yellow, PDB ID: 7VXY); (**b**) 2mFo-DFc (marine mesh, 1.0) electron-density map for the catalytic triad (His51-Asp75-Ser135) of the NS2B/NS3 protease.

4. Discussion

The BL17UM beamline at the SSRF is equipped with both a multilayer monochromator and a Si(111) monochromator. The Si(111) crystal and multilayer monochromator systems are mechanically switchable, enabling the consecutive use of two different beams with an energy resolution difference of almost two orders of magnitude. This dual setup option facilitates comparative studies of samples under two distinct beam characteristics. The multilayer system can achieve a 10-fold increase in flux density at 12.7 keV compared to the Si(111) monochromator, reaching levels similar to those in fourth-generation synchrotrons. This enhancement has enabled experiments with fluxes comparable to those of fourth-generation synchrotrons at a third-generation synchrotron.

As anticipated, the DMM facilitates faster data collection compared to the Si(111) monochromator. The shapes of spots in the lysozyme diffraction patterns exhibit streakiness similar to a previous study, in which a slightly wider bandpass multilayer (1.3%) resulted in streaky spots [3]. The observed streaky spots can be attributed to protein crystal mosaicity or the quality of the multilayer beam. The strong correlation in structure factors derived from the data collected with the two different monochromators indicates the equivalence of these structure factors. As anticipated, the lysozyme models obtained from the two datasets, solved through molecular replacement, resulted in the same model.

The protein crystal structures obtained at room temperature closely mimic their physiological states, providing more accurate structural information [34]. This is crucial for samples that may exhibit structural heterogeneity in cryogenic conditions [35]. However, there are challenges associated with collecting crystallographic data at room temperature, including radiation damage [36]. Additionally, data processing and analysis may be more complex, requiring more sophisticated methods [37]. We collected lysozyme crystal data using DMMs at room temperature and resolved the structure, which was consistent with the structure resolved by a DCM.

Integrating comparable, adequately cooled multilayer monochromators into third-generation sources can yield flux density improvements of over one order of magnitude, as demonstrated in the findings of this study. This enhancement can enable quicker measurements for screening or time-resolved studies, in which high flux densities are essential. Compared to traditional monochromators, the multilayer monochromator (DMM) provides stronger X-rays, making it an ideal choice for high-throughput crystallographic data collection at room temperature. In serial crystallography experiments, where crystals are often small with weak diffraction, the intense X-rays generated by DMMs significantly

improve the diffraction resolution, facilitating the acquisition of high-resolution structural information.

Despite the advantages of the higher beam intensity in macromolecular crystallography data collection using DMM, there are limitations and challenges. For proteins requiring heavy atoms for the determination of initial structures, the low energy resolution of DMM may result in weak anomalous scattering signals, making it challenging to resolve the phases of the protein structures. However, with the advancement of AlphaFold, the demand for heavy-atom initial structure determination has been alleviated using phase analysis through AlphaFold-generated structural models. The high accuracy of AlphaFold is anticipated to broaden the application of molecular replacement, potentially leading to a transition from SAD to AlphaFold-guided MR [38]. Additionally, the high divergence of DMM poses challenges in resolving protein structures with large unit cell parameters.

5. Conclusions

This study demonstrates the successful use of DMM for diffraction data collection and structure determination at the BL17UM beamline of the SSRF. Although slight streaking is observed in the diffraction patterns from DMM data, it does not impact protein structure determination. Comparing DMM-collected lysozyme crystal diffraction data with data collected using a Si(111) monochromator, we processed DMM data with standard software without parameter modification, revealing minor differences. Extending DMM applicability, diffraction data were collected and processed for SARS-CoV-2 Mpro and ZIKV NS2B/NS3, resolving their structures, which were consistent with those determined using a Si(111) monochromator. Additionally, crystal diffraction data were collected at room temperature, and the structure of a model protein was successfully resolved. These results offer valuable insights for scientists utilizing the DMM of the BL17UM beamline for life science research. The main innovation of this study is the successful resolving of the structures of a model protein and two important drug target proteins by using DMM at a third-generation synchrotron MX beamline in China.

Author Contributions: Conceptualization, H.Z. and Q.W.; Methodology, H.Z., F.Y. and Q.W.; Software, C.Z. and Q.X.; Validation, C.Z., Q.X., H.Z., W.W., M.L. (Miao Liang), M.L. (Minjun Li), L.Y., Z.Z., L.H., Q.L.and Y.W.; Formal analysis, C.Z. and Q.X.; Investigation, H.Z. and Q.W.; Resources, Q.W.; Data curation, C.Z. and Q.X.; Writing—original draft, C.Z. and Q.X.; Writing—review and editing, C.Z., Q.X., H.Z., W.W., M.L. (Miao Liang), M.L. (Minjun Li), L.Y., Z.Z., L.H., Q.L. and Y.W.; Visualization, C.Z. and Q.X.; Supervision, H.Z. and Q.W.; Funding acquisition, Q.W. All authors have read and agreed to the published version of the manuscript.

Funding: This work was supported by the Natural Science Foundation of Shanghai (21ZR1471800).

Data Availability Statement: The original contributions presented in the study are included in the article, and further inquiries can be directed to the corresponding authors.

Acknowledgments: The authors thank the teams at the BL17UM beamline of the Shanghai Synchrotron Radiation Facility and the User Experiment Assist System of the SSRF allocated to this project for the beamtime and for their help in experiments.

Conflicts of Interest: The authors declare no conflicts of interest.

References

1. Popov, A.M.; Dorovatovskii, P.V.; Mamichev, D.A.; Marchenkova, M.A.; Nikolaeva, A.Y. Development of a microfluidic chip for protein crystallization by the microbatch method. *Crystallogr. Rep.* **2019**, *64*, 282–286. [CrossRef]
2. Liebschner, D.; Dauter, M.; Rosenbaum, G.; Dauter, Z. How good can our beamlines be? *Acta Crystallogr. Sect. D Biol. Crystallogr.* **2012**, *68*, 1430–1436. [CrossRef]
3. Deacon, A.M.; Appleby, T.; Bilderback, D.H.; Ealick, S.E.; Fontes, E.; Thiel, D.J. Protein crystallography using a multilayer monochromator. *J. Synchrotron Radiat.* **1998**, *5*, 494–496. [CrossRef]
4. Knapp, G.S.; Beno, M.A. A new method to do time-resolved, x-ray-diffraction studies—The rotating crystal laue method. *Rev. Sci. Instrum.* **1992**, *63*, 1032–1034. [CrossRef]

5. Ren, Z.; Bourgeois, D.; Helliwell, J.R.; Moffat, K.; Srajer, V.; Stoddard, B.L. Laue crystallography: Coming of age. *J. Synchrotron Radiat.* **1999**, *6*, 891–917. [CrossRef]
6. Englich, U.; Kazimirov, A.; Shen, Q.; Bilderback, D.H.; Gruner, S.M.; Hao, Q. Crystallographic data collection using a 0.22% bandwidth multilayer. *J. Synchrotron Radiat.* **2005**, *12*, 345–348. [CrossRef]
7. Uesugi, K.; Hoshino, M.; Koyama, T.; Yamazaki, H.; Senba, Y.; Takeuchi, T.; Yumoto, H.; Ohashi, H.; Yamada, J.; Osaka, T.; et al. Demonstration of the x-ray imaging capabilities of the newly installed multilayer monochromator at spring-8 bl20b2. *J. Phys. Conf. Ser.* **2022**, *2380*, 012120. [CrossRef]
8. Kim, Y.; Nam, K.H. Pink-beam serial synchrotron crystallography at pohang light source ii. *Crystals* **2022**, *12*, 1637. [CrossRef]
9. Kneller, D.W.; Phillips, G.; Kovalevsky, A.; Coates, L. Room-temperature neutron and x-ray data collection of 3cl mprofrom SARS-CoV-2. *Acta Crystallogr. Sect. F Struct. Biol. Commun.* **2020**, *76*, 483–487. [CrossRef]
10. Schneps, C.M.; Ganguly, A.; Crane, B.R. Room-temperature serial synchrotron crystallography of drosophila cryptochrome. *Acta Crystallogr. Sect. D Struct. Biol.* **2022**, *78*, 975–985. [CrossRef]
11. Carrillo, M.; Mason, T.J.; Karpik, A.; Martiel, I.; Kepa, M.W.; McAuley, K.E.; Beale, J.H.; Padeste, C. Micro-structured polymer fixed targets for serial crystallography at synchrotrons and xfels. *IUCrJ* **2023**, *10*, 678–693. [CrossRef] [PubMed]
12. Pearson, A.R.; Mehrabi, P. Serial synchrotron crystallography for time-resolved structural biology. *Curr. Opin. Struct. Biol.* **2020**, *65*, 168–174. [CrossRef] [PubMed]
13. Soares, A.S.; Yamada, Y.; Jakoncic, J.; McSweeney, S.; Sweet, R.M.; Skinner, J.; Foadi, J.; Fuchs, M.R.; Schneider, D.K.; Shi, W.; et al. Serial crystallography with multi-stage merging of thousands of images. *Acta Crystallogr. Sect. F Struct. Biol. Commun.* **2022**, *78*, 281–288. [CrossRef]
14. Hough, M.A.; Owen, R.L. Serial synchrotron and xfel crystallography for studies of metalloprotein catalysis. *Curr. Opin. Struct. Biol.* **2021**, *71*, 232–238. [CrossRef] [PubMed]
15. Smith, K.M.L.; Panepucci, E.; Kaminski, J.W.; Aumonier, S.; Huang, C.-Y.; Eris, D.; Buntschu, D.; Meier, N.; Glettig, W.; McAuley, K.E.; et al. Sdu—Software for high-throughput automated data collection at the swiss light source. *J. Synchrotron Radiat.* **2023**, *30*, 538–545. [CrossRef] [PubMed]
16. Maveyraud, L.; Mourey, L. Protein x-ray crystallography and drug discovery. *Molecules* **2020**, *25*, 1030. [CrossRef] [PubMed]
17. Kaminski, J.W.; Vera, L.; Stegmann, D.P.; Vering, J.; Eris, D.; Smith, K.M.L.; Huang, C.Y.; Meier, N.; Steuber, J.; Wang, M.; et al. Fast fragment- and compound-screening pipeline at the swiss light source. *Acta Crystallogr. Sect. D Struct. Biol.* **2022**, *78*, 328–336. [CrossRef] [PubMed]
18. Weiss, M.S.; Wollenhaupt, J.; Correy, G.J.; Fraser, J.S.; Heine, A.; Klebe, G.; Krojer, T.; Thunnissen, M.; Pearce, N.M. Of problems and opportunities-how to treat and how to not treat crystallographic fragment screening data. *Protein Sci.* **2022**, *31*, e4391. [CrossRef]
19. Xu, Q.; Kong, H.-T.; Liu, K.; Zhou, H.; Zhang, K.-H.; Wang, W.-W.; Li, M.-J.; Pan, Q.-Y.; Wang, X.-Y.; Wang, Y.-Z.; et al. The biosafety level-2 macromolecular crystallography beamline (bl10u2) at the shanghai synchrotron radiation facility. *Nucl. Sci. Tech.* **2023**, *34*, 202. [CrossRef]
20. Liu, K.; Zhou, H.; Xu, Q.; Kong, H.-T.; Zhang, K.-H.; Wang, W.-W.; Li, M.-J.; Wang, Z.-J.; Pan, Q.-Y.; Wang, X.-Y.; et al. Bl02u1: The relocated macromolecular crystallography beamline at the shanghai synchrotron radiation facility. *Nucl. Sci. Tech.* **2023**, *34*, 193. [CrossRef]
21. Sun, B.; Wang, Y.Z.; Liu, K.; Wang, Q.S.; He, J.H. Design of new sub-micron protein crystallography beamline at ssrf. In Proceedings of the 13th International Conference on Synchrotron Radiation Instrumentation (SRI2018), Taipei, Taiwan, 11–16 June 2018; Volume 2054.
22. Hill, C.P.; Johnston, N.L.; Cohen, R.E. Crystal-structure of a ubiquitin-dependent degradation substrate—A 3-disulfide form of lysozyme. *Proc. Natl. Acad. Sci. USA* **1993**, *90*, 4136–4140. [CrossRef] [PubMed]
23. Ren, P.; Li, H.; Nie, T.; Jian, X.; Yu, C.; Li, J.; Su, H.; Zhang, X.; Li, S.; Yang, X.; et al. Discovery and mechanism study of SARS-CoV-2 3c-like protease inhibitors with a new reactive group. *J. Med. Chem.* **2023**, *66*, 12266–12283. [CrossRef] [PubMed]
24. Xiong, Y.; Cheng, F.; Zhang, J.; Su, H.; Hu, H.; Zou, Y.; Li, M.; Xu, Y. Structure-based design of a novel inhibitor of the zika virus ns2b/ns3 protease. *Bioorg. Chem.* **2022**, *128*, 106109. [CrossRef] [PubMed]
25. Kabsch, W. Xds. Acta Crystallogr. *Sect. D Biol. Crystallogr.* **2010**, *66*, 125–132. [CrossRef] [PubMed]
26. Emsley, P.; Cowtan, K. Coot: Model-building tools for molecular graphics. *Acta Crystallogr. Sect. D Struct. Biol.* **2004**, *60*, 2126–2132. [CrossRef] [PubMed]
27. Adams, P.D.; Afonine, P.V.; Bunkoczi, G.; Chen, V.B.; Davis, I.W.; Echols, N.; Headd, J.J.; Hung, L.-W.; Kapral, G.J.; Grosse-Kunstleve, R.W.; et al. Phenix: A comprehensive python-based system for macromolecular structure solution. *Acta Crystallogr. Sect. D Struct. Biol.* **2010**, *66*, 213–221. [CrossRef] [PubMed]
28. Afonine, P.V.; Grosse-Kunstleve, R.W.; Echols, N.; Headd, J.J.; Moriarty, N.W.; Mustyakimov, M.; Terwilliger, T.C.; Urzhumtsev, A.; Zwart, P.H.; Adams, P.D. Towards automated crystallographic structure refinement with phenix.Refine. *Acta Crystallogr. Sect. D Struct. Biol.* **2012**, *68*, 352–367. [CrossRef]
29. Nguyen, T.H.; Thai, Q.M.; Pham, M.Q.; Minh, P.T.H.; Phung, H.T.T. Machine learning combines atomistic simulations to predict SARS-CoV-2 mpro inhibitors from natural compounds. *Mol. Divers.* **2023**, *564*, 111709. [CrossRef]
30. Duan, Y.K.; Wang, H.F.; Yuan, Z.H.; Yang, H.T. Structural biology of SARS-CoV-2 mpro and drug discovery. *Curr. Opin. Struct. Biol.* **2023**, *82*, 102667. [CrossRef]

31. Jin, Z.M.; Du, X.Y.; Xu, Y.C.; Deng, Y.Q.; Liu, M.Q.; Zhao, Y.; Zhang, B.; Li, X.F.; Zhang, L.K.; Peng, C.; et al. Structure of mpro from SARS-CoV-2 and discovery of its inhibitors. *Nature* **2020**, *582*, 289–293. [CrossRef] [PubMed]
32. Hilgenfeld, R. From sars to mers: Crystallographic studies on coronaviral proteases enable antiviral drug design. *FEBS J.* **2014**, *281*, 4085–4096. [CrossRef] [PubMed]
33. Ghasemlou, A.; Uskokovic, V.; Sefidbakht, Y. Exploration of potential inhibitors for SARS-CoV-2 mpro considering its mutants via structure-based drug design, molecular docking, md simulations, mm/pbsa, and dft calculations. *Biotechnol. Appl. Biochem.* **2023**, *70*, 439–457. [CrossRef] [PubMed]
34. Aplin, C.; Milano, S.K.; Zielinski, K.A.; Pollack, L.; Cerione, R.A. Evolving experimental techniques for structure-based drug design. *J. Phys. Chem. B* **2022**, *126*, 6599–6607. [CrossRef]
35. Cellini, A.; Wahlgren, W.Y.; Henry, L.; Pandey, S.; Ghosh, S.; Castillon, L.; Claesson, E.; Takala, H.; Kubel, J.; Nimmrich, A.; et al. The three-dimensional structure of drosophila melanogaster (6-4) photolyase at room temperature. *Acta Crystallogr. Sect. D Struct. Biol.* **2021**, *77*, 1001–1009. [CrossRef] [PubMed]
36. Yabukarski, F.; Doukov, T.; Mokhtari, D.A.; Du, S.; Herschlag, D. Evaluating the impact of x-ray damage on conformational heterogeneity in room-temperature (277 k) and cryo-cooled protein crystals. *Acta Crystallogr. Sect. D Struct. Biol.* **2022**, *78*, 945–963. [CrossRef]
37. Thorne, R.E. Determining biomolecular structures near room temperature using x-ray crystallography: Concepts, methods and future optimization. *Acta Crystallogr. Sect. D Struct. Biol.* **2023**, *79*, 78–94. [CrossRef]
38. Hendrickson, W.A. Facing the phase problem. *IUCrJ* **2023**, *10*, 521–543. [CrossRef]